energies

MDPI

Article

A Simple Analytical Model of Static Eccentricity for PM Brushless Motors and Validation through FEM Analysis

Andrea Del Pizzo, Luigi Pio Di Noia and Emanuele Fedele *

Deptartment of Electrical Engineering and Information Technology, University of Naples Federico II, 80125 Napoli, Italy; andrea.delpizzo@unina.it (A.D.P.); luigipio.dinoia@unina.it (L.P.D.N.)

* Correspondence: emanuele.fedele@unina.it; Tel.: +39-081-768-3631

Received: 28 April 2020; Accepted: 29 June 2020; Published: 2 July 2020

Abstract: The paper firstly summarizes a simple analytical model of the air gap flux-density distribution for isotropic permanent magnet (PM) synchronous machines, in the presence of static eccentricity. The model was proposed by the authors in a previous paper and is based on an efficacious analytical expression of the variable length of air gap magnetic field lines which occur in eccentric brushless machines with surface-mounted permanent magnets. The approximate expression of the air gap field makes it possible to achieve a mathematical model with concentrated parameters close to that of a PM machine without eccentricity. The expression of the armature voltages and electromagnetic torque are found, also with reference to steady-state operating conditions at fixed rotor speed and impressed currents. The differences introduced by the considered type of eccentricity are evaluated and highlighted especially with reference to the air gap inductance and to waveforms and frequency spectra of voltages and shaft torque. Numerical results in a case-study of an 8-pole, 110 kW PM motor are compared to those obtained by using finite element analysis.

Keywords: static eccentricity; isotropic PM brushless machines; air gap flux-density

1. Introduction

Eccentricity is one of the widely diffused unexpected working conditions in electrical machines. When an eccentricity anomaly occurs in a machine, the length of the air gap between rotor and stator has a non-uniform distribution. As is well known, if the rotation axis of the rotor is fixed in time and parallel to that of the stator, the eccentricity is called "static"; otherwise it is named "dynamic". Many technical papers in literature deal with the study of the effects of eccentricity in induction machines' performance [1,2].

In the last two decades, brushless drives have largely been used due to the necessity to increase the power density and the overall efficiency of electric drives. Also, for this type of electric machine, eccentricity is one of the most common faults [3,4]. Regarding the study of the behavior of brushless electrical machines in the presence of eccentricity, some researchers are oriented to identifying anomalies during operation using mechanical vibrations and related noise [5]. Other authors proposed novel approaches based on stator current signatures [6].

The study of eccentricity effects using finite element analysis (FEA) is proposed in [7,8]; these techniques are characterized by accurate results, but the high computational cost is not always compatible for use in a real-time diagnostic process.

An analytical approach appears more useful for the diagnosis of eccentricity; different methodologies are applied in the literature [9–12] in order to develop an accurate mathematical model suitable for correctly taking eccentricity into account.

With the aim to reduce the complexity of the models, it is possible to introduce some simplifying hypotheses on the length of magnetic flux-density in the air gap and on the magnetization law of the permanent magnets [13,14]. Using these assumptions, in the paper the authors deepen a simplified mathematical model, already introduced in [15], capable of simulating the effects of static eccentricity. Referring to PM motors with surface-mounted permanent magnets, the paper is focused on the comparison between waveforms and spectra of some relevant quantities evaluated with and without static eccentricity. The results of the model are verified by means of finite element method (FEM) analysis in terms of no-load electromotive force (e.m.f.) and armature voltages and electromagnetic torque in an assigned steady state condition with impressed armature currents.

2. Introductory Elements for Static Eccentricity Analysis

2.1. Type of Motor under Analysis

The analysis of the effects of static eccentricity is carried out on isotropic radial-flux brushless motors, with surface-mounted magnets (Figure 1), which cover about 75–90% of the pole pitch.

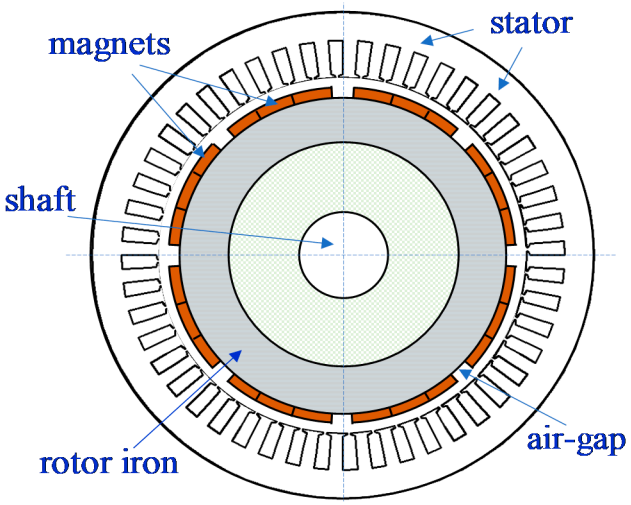

Figure 1. Cross-section of the considered type of permanent magnet (PM) motor.

The symmetrical three-phase stator winding is of *distributed* type (more than one slot per pole and per phase); the coils of each phase are all considered in series.

2.2. Basics of the Analytical Approach to the Study of Static Eccentricity

The stator and rotor iron surfaces facing the air gap are assumed to be cylindrical. Under the usual simplifying hypotheses in motor modeling, in ordinary (non eccentric) conditions, the magnetic field lines in the air gap are radial and with constant length $\delta_0 = R_s - R_r$ (Figure 2a).

In the presence of static eccentricity, the stator and rotor axes are no longer coincident, but parallel with a distance d (Figure 2b) and remain fixed over time during rotor rotation. As is known, eccentricity is the quantity usually defined as $\varepsilon = d/\delta_0$.

Considering a generic point P on the internal surface of the stator, from Figure 2b we can easily deduce that the segments PP′ (along the stator radius OsP) and PP″ (along the rotor radius OrP) are practically coincident. So, according to [15], we can consider the segments of PP′ type as approximated paths of the flux-density lines in the air gap, also called the magnetic air gap. Obviously, they are perpendicular only to the stator surface.

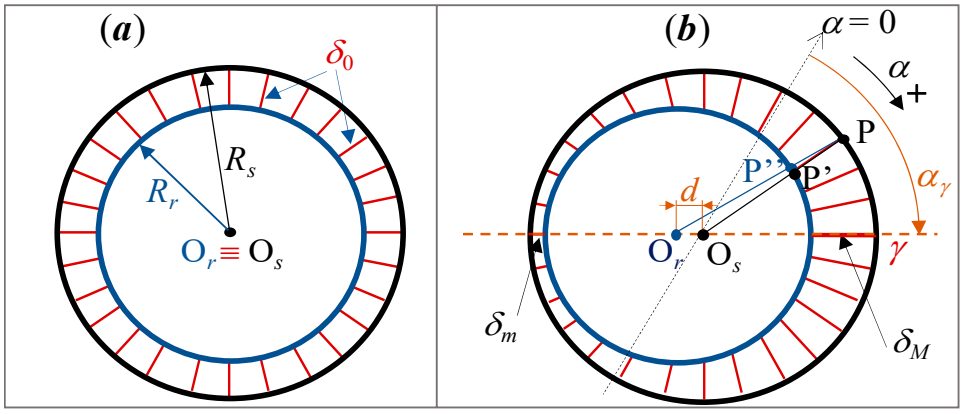

Figure 2. Schematic cross section of the considered PM motor type, without (**a**) and with (**b**) rotor static eccentricity.

The length δ of the air gap is then variable along a stator angular abscissa α, with a minimum ($\delta_m = \delta_0 - \varepsilon$) and a maximum ($\delta_M = \delta_0 + \varepsilon$) value along the straight line γ. Referring to Figure 2b, where the size of the air gap is magnified for greater clarity, the segment PP′ can be calculated as:

$$\mathrm{PP}' = \delta(\alpha) = R_s - \left[\sqrt{R_r^2 - d^2 \sin^2(\alpha - \alpha_\gamma)} - d\cos(\alpha - \alpha_\gamma)\right] \quad (1)$$

where α_γ is the angular position of γ, as shown in Figure 2b.

With the hypothesis that $d^2 << {R_r}^2$, Equation (1) becomes:

$$\mathrm{PP}' = \delta(\alpha) = R_s - R_r + d\cos(\alpha - \alpha_\gamma) = \delta_0 + d\cos(\alpha - \alpha_\gamma) \quad (2)$$

Using the above definition of eccentricity, the variable length of the air gap can be written as:

$$\delta(\alpha) = \delta_0 \left[1 + \varepsilon \cos(\alpha - \alpha_\gamma)\right] \quad (3)$$

In ordinary conditions the air gap magnetic permeance is constant and equal to $g_0 = 1/\delta_0$; when eccentricity is present, the permeance is a function of α and does not depend on the angular position of the rotor:

$$\lambda(\alpha) = \frac{1}{\delta(\alpha)} = \frac{1}{\delta_0 \left[1 + \varepsilon \cos(\alpha - \alpha_\gamma)\right]}. \quad (4)$$

The expansion in Fourier series of $\lambda(\alpha)$ is:

$$\lambda(\alpha) = \sum_{h=-\infty}^{\infty} \lambda_h \, e^{j\,h\,(\alpha - \alpha_\gamma)} \quad (5)$$

as shown in [15], the permeance in p.u. becomes:

$$\frac{\lambda(\alpha)}{\lambda_0} \cong 1 + \sum_{\substack{h=-\infty \\ h \neq 0}}^{\infty} \left(-\frac{\varepsilon}{2}\right)^{|h|} \cos[\,h\,(\alpha - \alpha_\gamma)] \quad (6)$$

where the average value λ_0 is equal to $\lambda_0 = \frac{1}{\delta_0 \sqrt{1-\varepsilon^2}} = \frac{g_0}{\sqrt{1-\varepsilon^2}}$, which is a little higher than g_0. From a physical point of view, the average value λ_0 gives the permeance of an electric motor without eccentricity and with an equivalent permeance equal to that of the faulty motor. Of course, this is true

only when the higher order harmonics of the permeance can be neglected, e.g., in the case of very low values of ε.

The coefficients of the series (5), in p.u. are equal to:

$$\frac{\lambda_h}{\lambda_0} = \lambda_h^{pu} = \frac{(-1)^{|h|}\left(1 - \sqrt{1-\varepsilon^2}\right)^{|h|}}{\varepsilon^{|h|}} \cong \left(-\frac{\varepsilon}{2}\right)^{|h|}; \tag{7}$$

from which: $\lambda_h^{pu} \cong (-\varepsilon_2)^{|h|}$ with $\varepsilon_2 = \varepsilon/2$. Usually few terms of the sum (5) are enough for an acceptable approximation.

In order to highlight how the air gap permeance is modified by the static eccentricity compared to the ordinary condition, Figure 3 shows a qualitative behavior of $\lambda(\alpha)/g_0$ for assigned values of ε and α_λ ($\varepsilon = 0.25$, $\alpha_\lambda = \pi/2$). In the figure the higher value of $\overline{\lambda}$ with respect to g_0 is also represented.

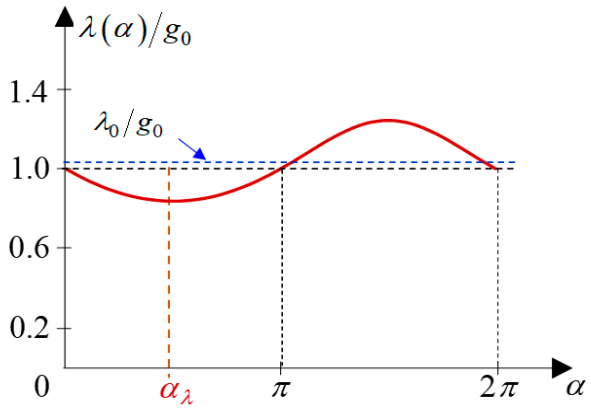

Figure 3. Air gap permeance referred to g_0; case $\varepsilon = 0.25$; $\alpha_\lambda = \pi/2$.

3. Air Gap Magnetic Flux-Density

3.1. Armature Flux-Density in the Air Gap

As already explained in [15], by taking into account the permeance expression (6) and neglecting iron losses and magnetomotive force (m.m.f.) drops in all iron paths, the instantaneous distribution $B_s(\alpha, t)$ along α of the flux-density generated in the air gap by a stator 3-*ph* system of currents can be expressed by:

$$B_s(\alpha, t) = \mu_0 \, \Delta F_s(\alpha, t) \, \lambda(\alpha, t) \tag{8}$$

Expliciting the m.m.f. drops and using (3), the relation (6) becomes:

$$B_s(\alpha, t) = \Re e\left\{\sum_{n=1}^{\infty} \mathbf{B}_{s,n}(t) \cdot \sum_{h=-\infty}^{\infty} \lambda_h^{pu}\left[e^{-j\,h\,\alpha_\lambda}\, e^{-j\,(p\,n-h)\,\alpha} - \lambda_h^{pu}\, e^{-j\,(p\,n+h)\,\alpha_\lambda}\, e^{j\,h\,\alpha}\right]\right\} \tag{9}$$

with:

- p pole-pair number;
- α stator angular abscissa, clockwise oriented, with $\alpha = 0$ on the magnetic axis of the 1st phase under the 1st pole-pair;
- $\Delta F_s(\alpha, t)$ air gap m.m.f. drop due to the stator currents;
- a wye-connected 3-*ph* winding, whose p coils of each phase are all in series.

Moreover, in (6) the term $\mathbf{B}_{s,n}(t)$, which is dimensionally a flux-density, is given by:

$$\mathbf{B}_{s,n}(t) = \frac{3\,\mu_0\,N\,\xi_1}{\pi\,p}\,\overline{\lambda}\,q_n\,\mathbf{i}_n(t), \tag{10}$$

where:

- n is an index equal to 1 and ($6\nu \pm 1$) with $\nu \in (1,\infty)$; i. e. $n = 1, 5, 7, 11, 13, \ldots$;
- N is the number of turns in series per phase;
- $_n$ is the winding-factor for the n^{th} spatial harmonic;
- q_n is a coefficient equal to: $q_n = \frac{1}{n}(-1)^{\frac{n-1}{2}} \frac{\xi_n}{\xi_1}$;
- $\mathbf{i}_n(t) = \mathbf{i}(t)$ for $n = 1, 7, 13, \ldots$; $\mathbf{i}_n(t) = \overset{\vee}{\mathbf{i}}(t)$ for $n = 5, 11, \ldots$;
- $\mathbf{i}\ (t)$ is the instantaneous currents space-vector equal to: $\mathbf{i}\ (t) = \frac{2}{3} \sum_{k=1}^{3} i_k(t)\ e^{j\ 2\ \pi(k-1)/3}$;
- $i_k(t)$ is the instantaneous current value in the k^{th} phase.

From Equation (9) we can deduce that the various terms depend on the quantities $p\ n \pm h$ and, for some of them, only the λ coefficients of order pn exist.

As a sample, Figure 4 shows the behavior along α of the flux-density $B_s(\alpha,t)$ generated by one stator phase current (e.g., $i_1(t)$) at its rated value. The case of a PM-motor with 8 poles and 48 armature slots is considered: magnitude and position of the eccentricity are respectively $\varepsilon = 0.25$ and $\alpha_\lambda = \pi/2$. More detailed parameters of the motor are reported in Section III.B, Table 1. The variability of the magnetic permeance can be deduced easily from the upper and lower envelopes of the flux-density curve which replicates the permeance behavior of Figure 3. The quantity $B_M{}^*$ in Figure 4 is the maximum flux-density value of one stator phase in the healthy non eccentric condition.

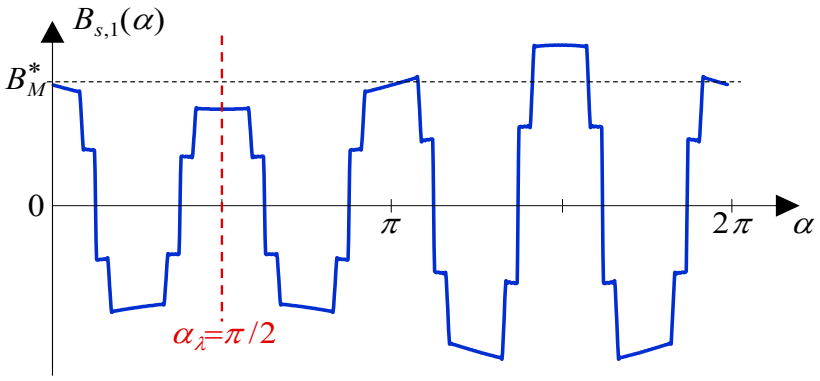

Figure 4. Air gap flux-density due to the 1st phase of armature for an 8-poles, 3-*ph* PM motor with $\varepsilon = 0.25$; $\alpha_\lambda = \pi/2$.

Table 1. Main motor parameters.

Rated power	110 kW	External rotor diameter	406 mm
Rated voltage	400 V	Polar arc/polar pitch (τ_a/τ_p)	0.88
Pole pairs	4	Type of magnets	N45UH
Number of stator slots	48	Remanence B_{re} at 100 °C	1.28 T
Internal stator diameter	320 mm	Coercitivity at 100 °C	955 kA/m
Geometric air gap length	2 mm	Magnet thickness l_m	5 mm

The armature linear current density $\Theta_s\ (\alpha, t)$ can be deduced from the air gap m.m.f. drop $\Delta F_s\ (\alpha, t)$ in (9):

$$\Theta_s\ (\alpha, t) = \frac{\mathrm{d}}{\mathrm{d}\alpha} \Delta F_s\ (\alpha, t) = \frac{3\ N\ \xi_1}{\pi}\ \Im m \left\{ \sum_{\nu=1}^{\infty} \nu\ q_\nu\ \mathbf{i}_\nu(t)\ e^{-j\ p\ \nu\ \alpha} \right\} \tag{11}$$

both $\Delta F_s\ (\alpha, t)$ and $\Theta_s\ (\alpha, t)$ are not dependent on the eccentricity. The quantity $\Theta_s\ (\alpha, t)$ is useful for the torque evaluation.

3.2. Rotor Flux-Density in the Air Gap

We assume that the remanence in rotor magnets is a generic $B_{Re}(\beta)$ symmetrical and periodic function of the rotor angular abscissa β, which has clockwise orientation and origin $\beta = 0$ on a polar axis. The air gap field-lines generated by the rotor magnets are assumed to coincide with those of the stator as in Figure 2b. Consequently, the rotor magnets work on circuits with variable permeance not only along β for a fixed position ϑ, but also over time for each fixed point at the abscissa β. Obviously, at constant speed ω_r, the ϑ position of the rotor is a linear function of time:

$$\vartheta = \alpha - \beta = \omega_r t + \vartheta_0, \tag{12}$$

where ϑ_0 is the angle between the α and β axes at instant 0. According to the hypotheses introduced in [15], the flux-density in the air gap is assumed constant along each field-line in Figure 2b. Since in rotor coordinates the length of these lines is $\delta(\alpha) = \delta(\beta + \vartheta)$, denoting with l_m the radial length of the magnets, the $B_r(\beta,\vartheta)$ flux-density generated by the rotor magnets in the air gap is linked to the remanence $B_{Re}(\beta)$ through the expression:

$$B_r(\beta, \vartheta) = \frac{l_m}{\delta(\beta + \vartheta)} B_{Re}(\beta) + C_\vartheta, \tag{13}$$

where C_ϑ is constant for each ϑ rotor position; it can be evaluated imposing the magnetic field to be solenoidal.

Considering a generic magnetization function $B_{Re}(\beta)$, whose expansion in Fourier series is:

$$B_{Re}(\beta) = \sum_{n=1}^{\infty} B_{Re,n} \, \Re e\left\{ e^{-j p n \beta} \right\}, \text{ with } n = 1, 3, 5, \ldots \tag{14}$$

and referring to the expression of the air gap permeance (5), in stator coordinates the relation (13) becomes:

$$B_r(\alpha, \vartheta) = \Re e\left\{ \sum_{n=1}^{\infty} \mathbf{B}_{r,n}(\vartheta) \sum_{h=-\infty}^{\infty} \lambda_h^{pu} \left[e^{-j h \alpha_\lambda} e^{-j(pn-h)\alpha} - \lambda_{p\,n}^{pu} e^{-j(p\,n+h)\,\alpha_\lambda} e^{j h \alpha} \right] \right\}, \text{ with } n = 1, 3, 5 \ldots \tag{15}$$

where the coefficients λ_h^{pu} are given by (7) and:

$$\mathbf{B}_{r,n}(\vartheta) = l_m \overline{\lambda} B_{Re,n} e^{j p n \vartheta} \tag{16}$$

At first, we can consider the ideal case of magnets which generate perfectly sinusoidal air gap flux-density in the absence of eccentricity, i.e., only the coefficient $\mathbf{B}_{r,1}(\vartheta) \neq 0$ in (15). With reference to an 8-pole motor (see Table 1 for its rated values and main data) in which a static eccentricity is arisen with $\varepsilon = 0.25$, Figure 5 shows the flux-density curves for two arbitrary ϑ positions of the rotor, assuming $\alpha_\lambda = \pi/2$.

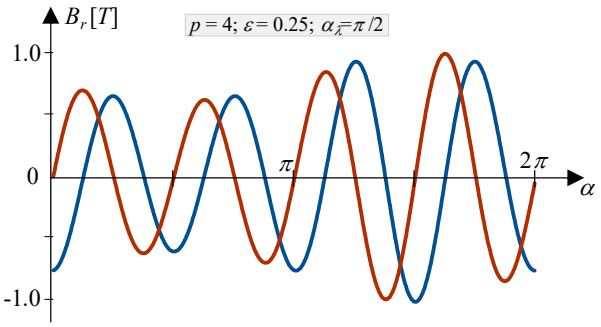

Figure 5. Sinusoidal magnetization of the magnets. Air gap flux-density due to the rotor magnets for $\vartheta_1 = \pi/4$ (blue line); $\vartheta_1 = \pi/8$ (red line).

As a second example, we can refer to the same motor of Table 1, but with different magnetization compared to the previous case. Figure 6 shows a pole pitch τ_p of the rotor; the magnets cover the τ_a polar arc and can be divided into some parts (three parts in the example); each of the latter is uniformly magnetized along radial directions. The value of the residual induction uniformly obtained in the magnets is assumed to be equal to 1.2 T at the temperature of 120 °C.

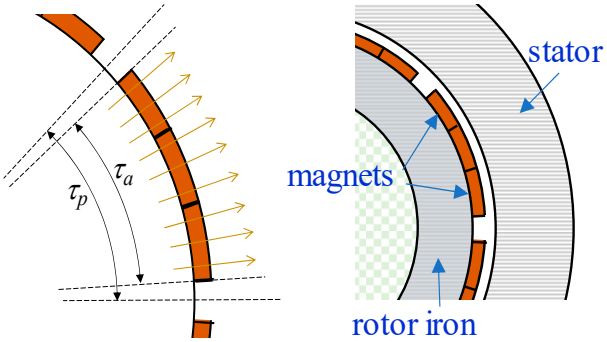

Figure 6. One pole pitch of the considered motor.

Figure 7 shows the field lines generated by rotor magnets in one pole of the considered motor of Table 1 in no-load operating conditions, neglecting the presence of the armature slots and assuming the iron permeability to be constant.

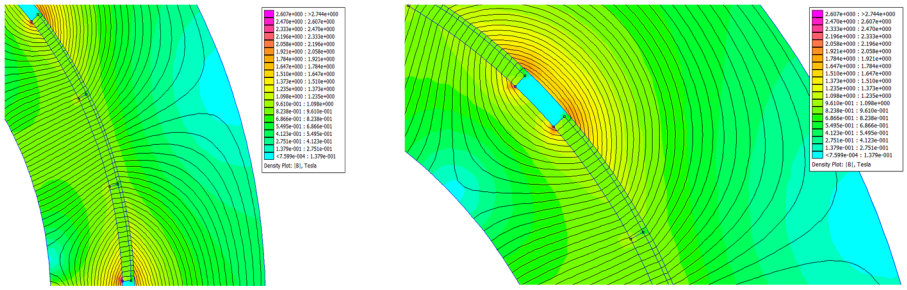

Figure 7. Two views of the rotor magnetic field in one motor pole.

The behavior along α of the flux-density $B_r(\alpha,\vartheta)$ is drawn in Figure 8, for an assigned ϑ position ($\vartheta = \pi/8\ rad$); the diagram (a) refers to the healthy case without eccentricity, while the diagram (b) shows the variations introduced by static eccentricity with $\varepsilon = 0.25$.

The diagrams of Figure 8 show a good match between the curves obtained theoretically or using FEM, in both cases without (a) and with (b) eccentricity. As can be seen from Figures 5 and 8, the static eccentricity significantly influences the air gap distribution of $B_r(\alpha,\vartheta)$ flux-density.

In both diagrams the curves obtained by FEM analysis (Appendix A) are drawn with solid blue lines, while brown dashed lines represent the results of Equations (15) and (16), with reference to an uniform remanence $B_{Re} = 1.2\ T$ in the magnets, that cover polar arcs of 88% of the pole pitch (see Table 1). As it is possible to note, the FEM analysis are carried out for a 2-D geometry, usually adopted for a radial flux motor. The 2-D CAD software neglects the behavior of end-windings and the edge effects of stator and rotor, but the end-windings are considered no-active magnetic parts of the motor (they affect only the leakage inductance value and the resistance calculation, and can be easily compensated introducing analytical corrections).

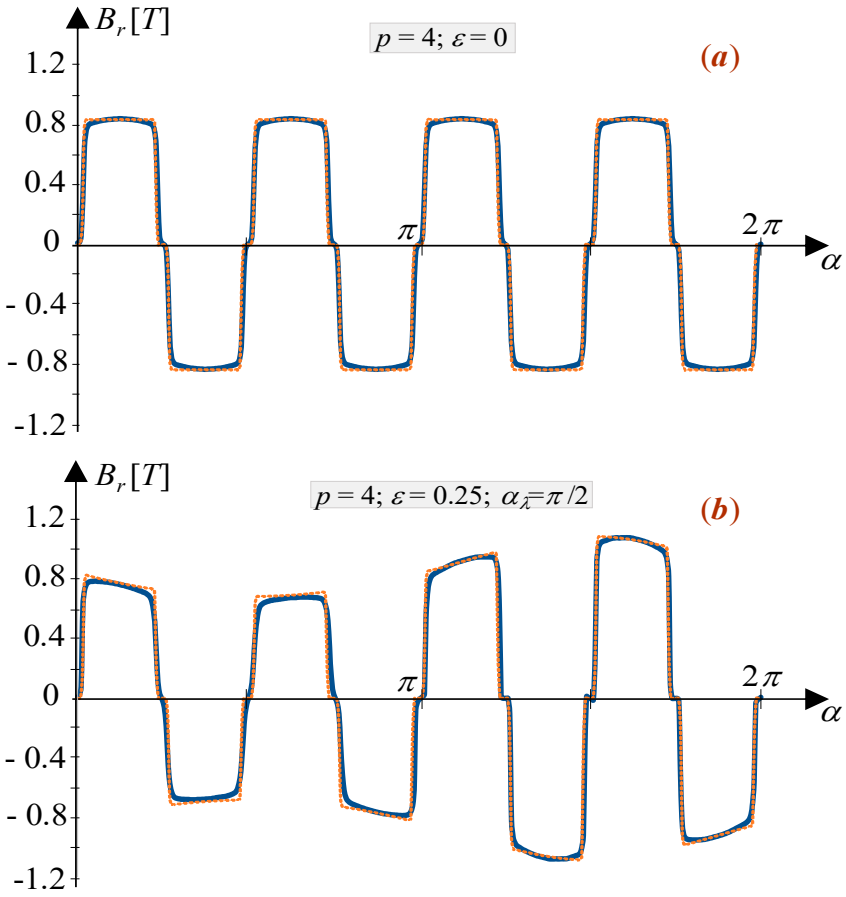

Figure 8. Radial uniform magnetization. Air gap flux-density due to rotor magnets without (**a**) or with (**b**) static eccentricity ($\varepsilon = 0.25$). The position assumed for the rotor is $\vartheta = \pi/8$. Theoretical result (*brown line*); FEM results (*blue line*).

3.3. Resultant Flux-Density in the Air Gap

The total air gap flux-density $B_\delta(\alpha, \vartheta)$ is obtained by adding the separate contributions of stator (6) and rotor (15), also considering that ϑ is the time-function (12); i.e.,:

$$B_\delta(\alpha,\ t) \ = \ B_s(\alpha,\ t) \ + \ B_r(\alpha, \vartheta)$$

$$B_\delta(\alpha,\ t) \ = \Re e, \left\{ \sum_{n=1}^{\infty} \mathbf{B}_{\delta,n}(t) \sum_{h=-\infty}^{\infty} (-\varepsilon_2)^{|h|} \cdot \left[\mathrm{e}^{-j\,h\,\alpha_\lambda}\, \mathrm{e}^{-j\,(p\,n-h)\alpha} - (-\varepsilon_2)^{p\,n} \mathrm{e}^{-j(p\,n+h)\,\alpha_\lambda}\, \mathrm{e}^{j\,h\,\alpha} \right] \right\} \tag{17}$$

where the coefficients $\mathbf{B}_{\delta,n}(t)$ are deduced from (10) and (16):

$$\mathbf{B}_{\delta,n}(t) \ = \ \mathbf{B}_{s,n}(t) + \ \mathbf{B}_{r,n}(\vartheta) \tag{18}$$

and where the approximated expression (7) of the p.u. permeance coefficients $\lambda_h{}^{pu}$ is used.

4. Induced Voltages and Armature Equations

With reference to the instantaneous values of the different quantities involved and neglecting the elasticity of the shaft, the mathematical model of the PM motor considered is composed by the set of equations:

$$\begin{cases} \mathbf{v} = R\,\mathbf{i} \ + L_{S,\varepsilon} \frac{\mathrm{d}\,\mathbf{i}}{\mathrm{d}\,t} \ + \ \mathbf{e}_{rot} \\ m_e - m_L = J\,\frac{\mathrm{d}\omega_r}{\mathrm{d}\,t} \end{cases} \tag{19}$$

where the different symbols represent:

- m_e—electromagnetic torque;
- m_L—load torque;
- ω_r—rotation speed;
- J—total rotor inertia;
- R—armature phase resistance;
- $L_{S,\varepsilon}$ synchronous inductance in presence of eccentricity, with $L_{S,\varepsilon} = L_\sigma + L_{m,\varepsilon}$;
- L_σ—armature phase leakage inductance;
- $L_{m,\varepsilon}$—air gap mutual inductance in presence of eccentricity;

the expression of $L_{m,\varepsilon}$ is given in [15] and here reported as:

$$L_{m,\varepsilon} = \frac{3\,\mu_0\,\overline{\lambda}\,D\,L\,N^2\xi_1^2}{\pi p^2}\sum_{n=1}^{\infty}\frac{1}{n^2}\,\frac{\xi_n^2}{\xi_1^2}\left(1\;-\;{\varepsilon_2}^{2p\;n}\right) \tag{20}$$

with $n = 1, 5, 7, 11, 13, \ldots$;

- D—internal diameter of the stator;
- L—motor length;
- I—instantaneous space vector of the armature current;
- **v**—instantaneous space vector of the armature voltage;
- $\mathbf{e}_{rot}$— instantaneous space vector of the back e.m.f. in stator windings due to the rotor magnets.

The aforementioned space vectors are equal to:

$$\begin{gathered}\mathbf{i}\,(t)\;=\;\tfrac{2}{3}\sum_{k=1}^{3}\,i_k\,(t)\,\mathrm{e}^{j\,2\,\pi(k-1)/3};\mathbf{v}\,(t)\;=\;\tfrac{2}{3}\sum_{k=1}^{3}\,v_k\,(t)\,\mathrm{e}^{j\,2\,\pi(k-1)/3}\\ \mathbf{e}_{rot}\,(t)\;=\;\tfrac{2}{3}\sum_{k=1}^{3}\,e_{rot,k}(t)\,\mathrm{e}^{j\,2\,\pi(k-1)/3}\end{gathered} \tag{21}$$

where $v_k(t)$ and $i_k(t)$ are instantaneous voltage and current values of the k^{th} armature phase; all the coils of each phase winding are considered in series.

Using this hypothesis, the back e.m.f. $e_{rot,k}\,(t)$ induced in the k^{th} stator phase by the rotor magnets is the sum of the back e.m.f. $e_{rot,k,\nu}\,(t)$ induced in the p coils of the considered phase:

$$e_{rot,k}(t)\;=\;\sum_{\gamma=\,1}^{p}\,e_{rot,k,\gamma}(t)\;=\;\sum_{\gamma=\,1}^{p}\frac{\mathrm{d}}{\mathrm{d}\,t}\,\phi_{k,\gamma}(t) \tag{22}$$

Obviously, if there is eccentricity, the different rotor fluxes $\phi_{k,\gamma}\,(t)$ (with $\gamma = 1, \ldots, p$) linked with the various $\gamma^{\,th}$ coils of the k^{th} phase are not equal, because of their different positions with respect to the axis λ in Figure 2b.

The expression of $\phi_{k,\gamma}\,(t)$ can be obtained by means a suitable integration of $B_r(\alpha,\;\vartheta)$ rotor flux-density (15). The final expression of $\phi_{k,\gamma}\,(t)$ (see also [15]) is:

$$\begin{gathered}\phi_{k,\gamma}(t) = \tfrac{DL}{2}\tfrac{N\xi_1}{p}\,\Re e\left\{\sum_{n=1}^{\infty}\tfrac{\xi_n}{\xi_1}\mathbf{B}_{r,n}(t)\sum_{h=\,-\infty}^{\infty}\lambda_h^{pu}\left[\tfrac{2}{pn-h}\,\mathrm{e}^{-j\,h\,\alpha_\lambda}\,\cdot\,\sin\!\left[(pn-h)\tfrac{\pi}{2p}\right]\mathrm{e}^{-j\,(pn-h)\,\frac{2\pi}{p}\,(\gamma-1)}\mathrm{e}^{-j\,(pn-h)\,\frac{2\pi}{3p}\,(k-1)}+\right.\right.\\ \left.\left.-\,\tfrac{2\,\lambda_{p\,n}^{pu}}{h}\,\mathrm{e}^{-j(p\,n+h)\,\alpha_\lambda}\sin\!\left(h\,\tfrac{\pi}{2p}\right)\mathrm{e}^{j\,h\,\frac{2\pi}{p}\,(\gamma-1)}\,\mathrm{e}^{j\,h\,\frac{2\pi}{3p}\,(k-1)}\right]\right\}.\end{gathered} \tag{23}$$

From (23) we deduce that only the rotor flux-density components of order equal to an odd multiple of p contribute to the $\phi_{k,\gamma}\,(t)$ flux linked with the $\gamma^{\,th}$ coil, while the terms are zero if h= pn or $h = 0$.

Moreover, by adding the various $\phi_{k,\gamma}\,(t)$ (for $\gamma = 1, \ldots, p$) in order to obtain the total flux $\phi_k\,(t)$ linked with the arbitrary k^{th} phase, many components introduced by eccentricity do not give

contribution to ϕ_k (t), even if present in the expression of the resulting air gap flux-density. Only the terms of $B_\delta(\alpha,\ t)$ with periodicity multiple of p contribute to ϕ_k (t).

Combining (22) and (23), the resulting $e_{rot,k}(t)$ can be expressed as:

$$e_{rot,k}(t) \ = \frac{D\,L\,N\,\xi_1}{p}\,\Re e\left\{\sum_{n=1}^{\infty}\frac{\mathrm{d}}{\mathrm{d}\,t}\mathbf{B}_{r,n}(t)\ q_n\ \cdot\left[1-\left(\lambda_{pn}^{pu}\right)^2\right]\mathrm{e}^{-j\ 2\pi\ n\ (k-1)/3}\right\} \tag{24}$$

Consequently, considering the $\mathbf{B}_{r,n}(t)$ expression (16), the $\mathbf{e}_{rot}$ (t) space-vector (21) is equal to:

$$\mathbf{e}_{rot}\ (t)\ =\ j\,p\,\omega_r\sum_{n\,=\,-\infty}^{\infty}\ (6n+1)\ \Phi_{r,|6n+1|}\ \mathrm{e}^{j\ (6n+1)p\ \vartheta}, \tag{25}$$

where ω_r is the instantaneous rotor speed with ω_r = $\mathrm{d}\vartheta/\mathrm{d}t$, and the rotor flux components have expression:

$$\Phi_{r,|6n+1|}=\ \frac{DL\,N\xi_1\,q_{|6n+1|}}{p}\left(1-\ \varepsilon_2^{2|6n+1|p}\right)l_m\ \overline{\lambda}\ B_{Re,|6n+1|}. \tag{26}$$

Based on the different quantities introduced in this section, the first equation of the set (19) can be written as:

$$\mathbf{v}=R\,\mathbf{i}\ +L_{S,\varepsilon}\frac{\mathrm{d}\,\mathbf{i}}{\mathrm{d}\,t}\ +\ jp\,\omega_r\sum_{n\,=\,-\infty}^{\infty}\ (6n+1)\ \Phi_{r,|6n+1|}\ \mathrm{e}^{j\ (6n+1)p\ \vartheta} \tag{27}$$

5. Electromagnetic Torque

The instantaneous electromagnetic torque developed by the motor can be evaluated by means of the well-known expression:

$$m_e(t)=\ \frac{D\,L}{2}\int_0^{2\pi}B_\delta(\alpha,t)\ \Theta_s\ (\alpha,t)\ \mathrm{d}\alpha \tag{28}$$

Replacing the $\Theta_s\ (\alpha,t)$ and $B_\delta(\alpha,t)$ quantities with their expressions (11) and (17) (without approximating λ_h^{pu}), we have:

$$m_e(t)=\ \frac{3\,D\,L\,N\xi_1}{4\,\pi}\ \Im m\ \{\mathbf{W}_1(t)\ +\ \mathbf{W}_2(t)\ \} \tag{29}$$

where $\mathbf{W}_1(t)$ and $\mathbf{W}_2(t)$ are separately evaluated below. For $\mathbf{W}_1(t)$:

$$\mathbf{W}_1(t)=\sum_{\nu=1}^{\infty}\sum_{n=1}^{\infty}\sum_{h=\,-\infty}^{\infty}\nu\,q_\nu\ \mathbf{i}_\nu(t)\ \mathbf{B}_{\delta,n}(t)\ \lambda_h^{pu}\int_0^{2\pi}\left[\mathrm{e}^{-j\ h\ \alpha_\lambda}\cdot\mathrm{e}^{-j\ (p\ n-h+p\ \nu)\ \alpha}-\ \lambda_{pn}^{pu}\ \mathrm{e}^{-j(p\ n+h)\ \alpha_\lambda}\ \mathrm{e}^{j\ (h-p\ \nu)\ \alpha}\right]\mathrm{d}\alpha \tag{30}$$

the non-null terms are only those with $h=\ p\ n+p\ \nu$ or $h=p\ \nu$; therefore, the previous equation can be written as:

$$\mathbf{W}_1(t)=\ 2\,\pi\sum_{\nu=1}^{\infty}\sum_{n=1}^{\infty}\ \nu\,q_\nu\ \mathbf{i}_\nu(t)\ \mathbf{B}_{\delta,n}(t)\ \dot{\Lambda}_{\nu,n} \tag{31}$$

where:

$$\dot{\Lambda}_{\nu,n}=\ \mathrm{e}^{-j\ p\ (\nu+n)\ \alpha_\lambda}\left[\lambda_{p(\nu+n)}^{pu}-\ \lambda_{p\ \nu}^{pu}\lambda_{p\ n}^{pu}\right] \tag{32}$$

since from (7) we can deduce that:

$$\lambda_{p\ \nu}^{pu}\ \lambda_{p\ n}^{pu}\ =\ \lambda_{p(\nu+n)}^{pu} \tag{33}$$

the quantity $\dot{\Lambda}_{\nu,n}$ is null and, consequently, also $\mathbf{W}_1(t)$ = 0.

Likewise, the quantity $\mathbf{W}_2(t)$ in (29) is expressed by:

$$\mathbf{W}_2(t) = -\sum_{\nu=1}^{\infty}\sum_{n=1}^{\infty}\sum_{h=-\infty}^{\infty} \nu\, q_\nu\, \overset{\vee}{\mathbf{i}}_\nu(t)\, \mathbf{B}_{\delta,n}(t)\, \lambda_h^{pu} \int_0^{2\pi} \left[\mathrm{e}^{-j\,h\,\alpha_\lambda}\cdot \mathrm{e}^{-j\,(p\,n-h-p\,\nu)\,\alpha} - \lambda_{pn}^{pu}\, \mathrm{e}^{-j(p\,n+h)\,\alpha_\lambda}\, \mathrm{e}^{j\,(h+p\,\nu)\,\alpha}\right] \mathrm{d}\alpha \tag{34}$$

In this case, the non-null terms are only those with $h = p\,(n-\nu)$ or $h = -p\,\nu$; therefore, the previous equation can be written as:

$$\mathbf{W}_2(t) = -2\,\pi \sum_{\nu=1}^{\infty}\sum_{n=1}^{\infty} \nu\, q_\nu\, \overset{\vee}{\mathbf{i}}_\nu(t)\, \mathbf{B}_{\delta,n}(t)\, \dot{\Gamma}_{\nu,n} \tag{35}$$

where:

$$\dot{\Gamma}_{\nu,n} = \mathrm{e}^{-j\,p\,(n-\nu)\,\alpha_\lambda}\left[\lambda_{p(n-\nu)}^{pu} - \lambda_{-p\,\nu}^{pu}\,\lambda_{p\,n}^{pu}\right] \tag{36}$$

from (7) we derive:

$$\dot{\Gamma}_{\nu,n} = \mathrm{e}^{-j\,p\,(n-\nu)\,\alpha_\lambda}\left[\lambda_{p(n-\nu)}^{pu} - \lambda_{p(n+\nu)}^{pu}\right] \tag{37}$$

Synthesizing the above considerations, the torque expression (29) becomes:

$$m_e(t) = -\frac{3\,N\xi_1\,D\,L}{2}\,\Im m\left\{\sum_{\nu=1}^{\infty}\sum_{n=1}^{\infty} \nu\, q_\nu\, \overset{\vee}{\mathbf{i}}_\nu(t)\, \mathbf{B}_{\delta,n}(t)\, \dot{\Gamma}_{\nu,n}\right\} \tag{38}$$

The air gap flux-density $\mathbf{B}_{\delta,n}(t)$ is the sum of the contributions of stator and rotor (see Equations (10), (16) and (18)), then the instantaneous torque $m_e(t)$ can be expressed as:

$$m_e(t) = m_{s,r}(t) + m_{s,s}(t) \tag{39}$$

(a) Interaction Stator–Rotor $[m_{s,r}(t)\,]$

The rate $m_{s,r}(t)$ of the torque can be obtained replacing in (31) the quantity $\mathbf{B}_{\delta,n}(t)$ with $\mathbf{B}_{r,n}(t)$ expressed by (16). Moreover, the terms with $n = \nu$ are separated from the others; we obtain:

$$m_{s,r}(t) = -\tfrac{3}{2}\,p\,\Im m\left\{\sum_{n=1}^{\infty} n\, \overset{\vee}{\mathbf{i}}_n(t)\, \Phi_{r,n}\, \mathrm{e}^{j\,p\,n\,\vartheta} + \sum_{\substack{\nu=1 \\ n\neq\nu}}^{\infty}\sum_{n=1}^{\infty} \tfrac{\nu\,q_\nu}{q_n\,\Gamma_{n,n}}\, \dot{\Gamma}_{\nu,n}\, \overset{\vee}{\mathbf{i}}_\nu(t)\, \Phi_{r,n}\, \mathrm{e}^{j\,p\,n\,\vartheta}\right\} \tag{40}$$

(b) Interaction Stator–Stator $[m_{s,s}(t)\,]$

The rate $m_{s,s}(t)$ of the torque is obviously due to the magnetic anisotropy introduced by eccentricity. It can be obtained replacing in (31) the quantity $\mathbf{B}_{\delta,n}(t)$ with $\mathbf{B}_{s,n}(t)$ expressed by (10), i.e.,:

$$m_{s,s}(t) = -\frac{3p}{2}\,L_{m,1}\,\Im m\left\{\sum_{\nu=1}^{\infty}\sum_{\substack{n=1 \\ n\neq\nu}}^{\infty} \nu\, q_\nu\, q_n\, \dot{\Gamma}_{\nu,n}\, \overset{\vee}{\mathbf{i}}_\nu(t)\, \mathbf{i}_n(t)\right\} \tag{41}$$

where $L_{m,1}$ is the air gap mutual inductance relating to the 1st spatial harmonic of the armature field in presence of eccentricity:

$$L_{m,1} = \frac{3\,\mu_0\,D\,L\,N^2\xi_1^2}{\pi\,p^2}\,\overline{\lambda} \tag{42}$$

For $\nu = n$, both the quantities $\overset{\vee}{\mathbf{i}}_{\nu}(t)\,\mathbf{i}_n(t) = \left|\mathbf{i}_n(t)\right|^2$ and $\dot{\Gamma}_{\nu,n} = \Gamma_n$ in (34) are real; consequently, their corresponding contribution to the torque is zero.

The resulting instantaneous torque is then the sum of (40) and (41).

6. Numerical Investigation

In this section, some numerical results of the model introduced above are compared with those obtained using analysis with finite elements methods. The results refer to the PM motor of Table 1, under steady state operating conditions at constant ω_r speed. In these conditions, the $e_{rot,k}(t)$ back e.m.f. (24) induced in the k^{th} phase of armature by the rotor flux-density $B_r(\alpha,\ \vartheta)$ can be expressed as:

$$e_{rot,k}(t) = \sqrt{2}\,\Re e\left\{\sum_{n=1}^{\infty}\mathbf{E}_n\,\mathrm{e}^{j\,n\,\omega\,t}\,\mathrm{e}^{-j\,2\pi n\,(k-1)/3}\right\} \tag{43}$$

where $\omega = p\,\omega_r$ is the fundamental angular frequency and the phasor $\mathbf{E}_n$ for the n^{th} harmonic of back e.m.f. is expressed by:

$$\mathbf{E}_n = \frac{1}{\sqrt{2}}\,j\,n\,\omega\,\Phi_{r,n}\,\mathrm{e}^{j\,n\,p\,\vartheta_0}\ \text{with}\ n = 1,\ 2,\ \ldots\ \infty. \tag{44}$$

The angle ϑ_0 is the position of the rotor at instant $t = 0$ (12), while $\Phi_{r,n}$ is the amplitude of the n^{th} harmonic of the rotor flux linked with a stator phase (26).

With reference to a rotor speed of 1500 rpm, Figure 9 shows the no-load induced voltage in an armature phase (diagram *a*) and the related frequency spectrum (b). The f_1 fundamental frequency of the induced voltage is 100 Hz. In the spectrum of Figure 9b the harmonic amplitudes are expressed in *p.u.* of the fundamental $\mathrm{E}_{1,\mathrm{FEM}}$ obtained in the FEM analysis. Blue lines refer to the results of FEM analysis obtained with the rotor flux-density in Figure 8; brown lines are used for the theoretical curves. An acceptable approximation can be observed, especially for the most significant harmonics.

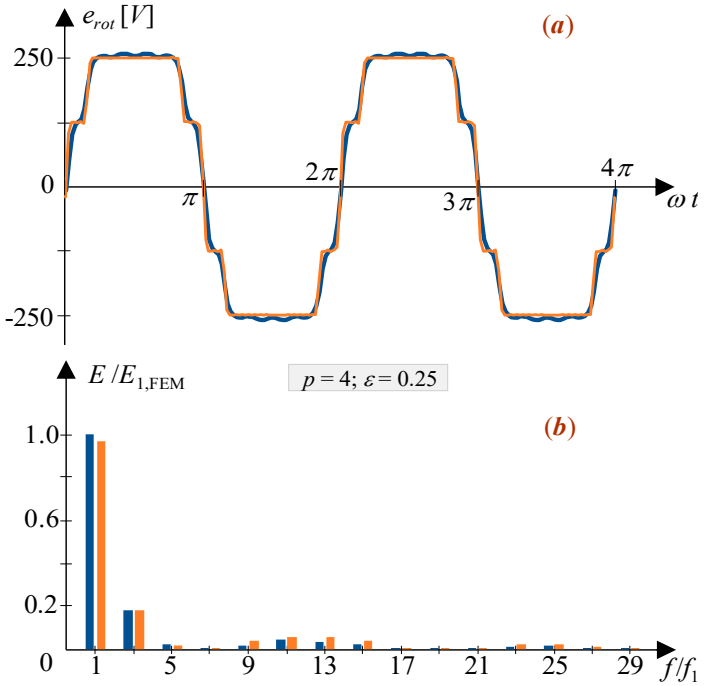

Figure 9. No-load voltage induced in a stator phase at 1500 rpm. (**a**) Time behavior; (**b**) amplitude frequency spectrum in p.u. Theoretical (brown line) and FEM values (blue line).

In order to evidence the variations introduced by static eccentricity, in Figure 10 the spectrum of the e.m.f. induced in a stator phase in the case of healthy (green line) is compared to the spectrum in presence of eccentricity (blue line), both obtained through FEM simulation; all harmonic amplitudes are in p.u. of the fundamental one in the healthy case.

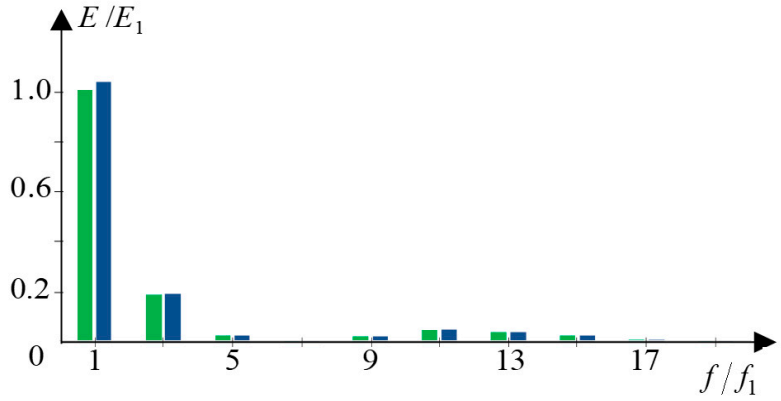

Figure 10. Comparison between no-load induced voltage in case of symmetric rotor (green line) and eccentric rotor (blue line).

The eccentricity does not introduce any harmonic of different order than those of the symmetric case; moreover the amplitudes of fundamental and other harmonics are a little higher (a few percent) when the eccentricity is present.

A load condition is examined with impressed armature currents. The latter are assumed to be symmetrical and sinusoidal with angular frequency $\omega = p\,\omega_r$, as occurs in the steady state operation of brushless AC drives controlled in feedback and with a current loop for motor feeding.

At steady state, the voltage **v** of Equation (27) can be written as:

$$\mathbf{v}\,(t) = \sum_{n=1}^{\infty} \mathbf{V}_n\, \mathrm{e}^{j\,n\,\omega\,t} \tag{45}$$

whose different $\mathbf{V}_n$ components can be evaluated through the equations:

$$\mathbf{V}_n = (R + j\,n\,\omega L_{S,\varepsilon})\,\mathbf{I}_n + \mathbf{E}_n, \text{ with } n = 1,\ 3,\ 5,\ \ldots \tag{46}$$

In (46) $\mathbf{E}_n$ is given by (44) and $\mathbf{I}_n = 0$ for $n \neq 1$, by hypothesis.

With reference to the motor of Table 1 in a load condition with rated armature currents, Figure 11 shows the waveforms of the three armature phase voltages; the diagram (*a*) refers to the voltages evaluated using FEM analysis, while the voltages draw in the diagram (*b*) are evaluated by means of the above presented model. The three voltages remain symmetrical, as predicted by the model; the two sets of curves (*a*) and (*b*) are quite similar. The same occurs for the corresponding frequency spectra shown in Figure 12.

The electromagnetic torque at steady state can be derived from (39), (40) and (41). The average value of the torque $M_{e,med}$ in a period $T = 2\pi/\omega$ can be approximated through the expression:

$$M_{e,med} = -\tfrac{3}{2} p\, \Im m \left\{ \underbrace{\overset{\vee}{\mathbf{I}}\, \Phi_{r,1} \left(1 + \dot{\sigma}_{7,1} + \dot{\sigma}_{13,1} + \ldots\right)}_{\text{(a)}} + \underbrace{I^2 \left(\dot{\rho}_{1,7} + \dot{\rho}_{1,13} + \ldots\right) + I^2 \left(\dot{\rho}_{5,11} + \dot{\rho}_{5,17} + \ldots\right) + \ldots}_{\text{(b)}} \right\} \tag{47}$$

where:

- $\mathbf{I} = I\, e^{\,j\,\varphi}$ is the phasor of the impressed sinusoidal armature current at angular frequency $\omega = p\,\omega_r$;
- $\Phi_{r,1} = \Phi_{r,1}\, e^{\,j\,p\vartheta_0}$ is the phasor of the fundamental harmonic of the rotor flux linked with the armature winding;
- the complex coefficients $\dot{\sigma}_{\nu,1}$ and $\dot{\rho}_{\nu,n}$, derived respectively from (40) and (41), are equal to:

$$\dot{\sigma}_{\nu,1} = \frac{\nu\, q_\nu\, \dot{\Gamma}_{\nu,1}}{q_1\, \Gamma_{1,1}};\ \dot{\rho}_{\nu,n} = \nu\, q_\nu\, q_n\, \dot{\Gamma}_{\nu,n} \tag{48}$$

The term (a) in (46) is extracted from (40) and represents the contribution to the average torque due to the interaction between stator and rotor fields. The term (b) is extracted by (41) and depends only by the armature currents. Compared to the healthy case, the eccentricity slightly changes the term $\mathbf{\Phi}_{r,1}$ and all the various $\dot{\sigma}_{\nu,1}$; however, the contribution of the latter terms is very low. The air gap magnetic anisotropy introduced by eccentricity gives rise to the term (b), whose contribution to the average torque is also quite modest and can generally be neglected.

By analyzing Equation (40) at steady state, some sinusoidal components of the torque can be deduced at angular frequency 6ω, 12ω, ... They depend on the interaction between the spatial harmonics of the linear current density and the spatial harmonics of the rotor field in the air-gap. Their analytical expressions are here omitted for simplicity, also because the magnitude of these components is not significantly different from those in the absence of anisotropy. Moreover, Equation (41) at steady state yields additional sinusoidal torque components at angular frequency 2ω due to the magnetic anisotropy caused by eccentricity. However, the amplitude of these components is very small and can be neglected.

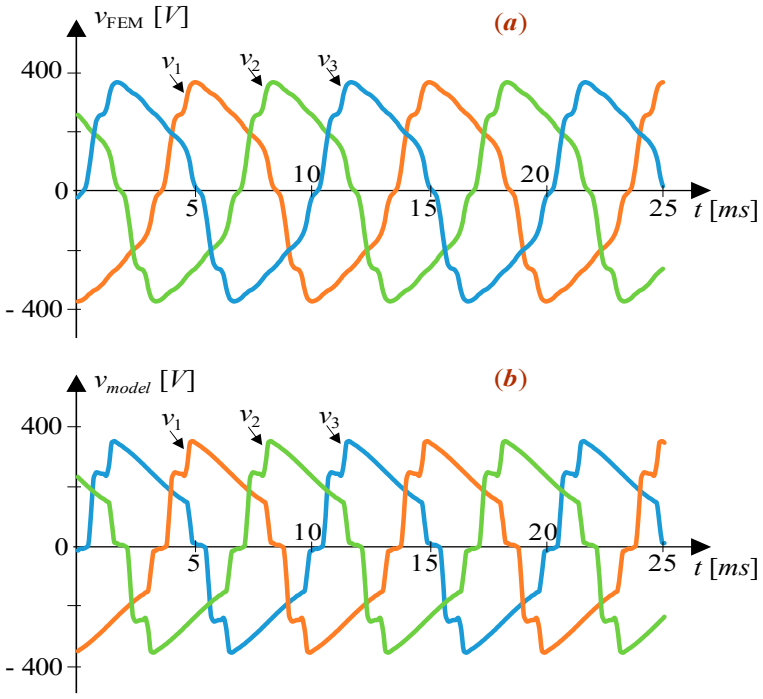

Figure 11. Armature voltages in rated load conditions at steady state; (**a**) results of FEM analysis; (**b**) results from theoretical model.

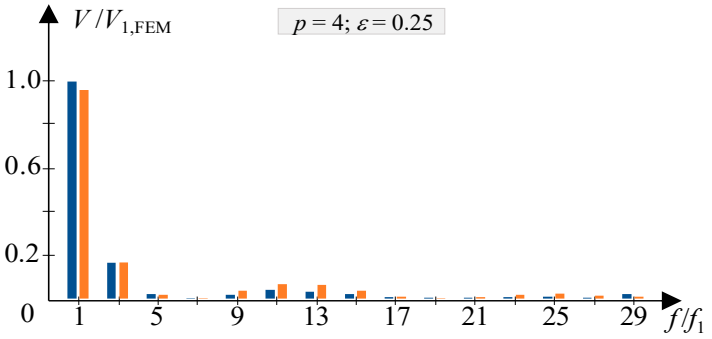

Figure 12. Amplitude (*p.u.*.) frequency spectrum of the phase voltage Theoretical (brown line) and FEM values (blue line).

With reference to the rated steady state operating condition, the electromagnetic torque is plotted as a function of the time in Figure 13a, where the waveform evaluated with the model equations (brown line) is compared with that obtained by the FEM analysis (blue line); the figure shows also the instantaneous torque in non-eccentric case (gray line). A magnification of a section allows to better highlight the differences between the three curves. The spectrum of the torque is shown in Figure 13b; the amplitude values are expressed in p.u. of the average value $M_{e,med}$ evaluated by FEM in the healthy non-eccentric case. Only harmonics of order $6n$ are visible, even if all of them are very small with respect to the torque average value. Also in this case there is a good correspondence between the results of the model and those of FEM analysis. In broad terms, we can notice that eccentricity does not modify the shape of the instantaneous torque but slightly increases its average value.

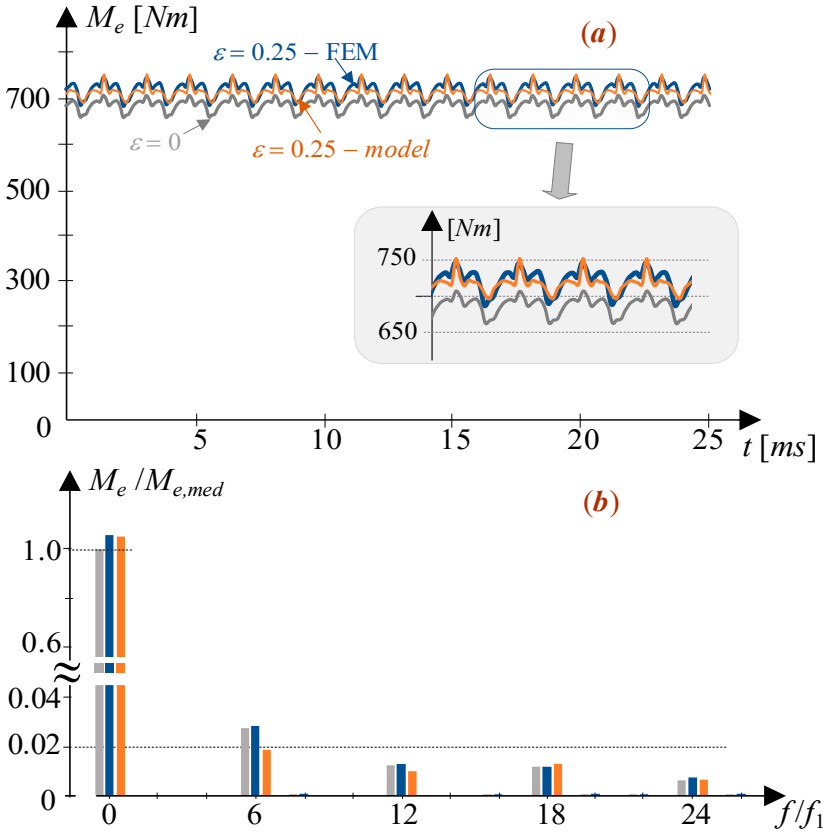

Figure 13. Motor electromagnetic torque. (**a**) Time waveform; (**b**) frequency spectrum. FEM analysis (blue and gray line) and model results (brown line).

Finally, for the motor considered in the case-study, the expression (20) of the air gap mutual inductance $L_{m,\varepsilon}$ is plotted in Figure 14 as a function of the eccentricity ε (brown line) and is compared with the results of the evaluation through FEM analysis (blue line). A very slight increase of $L_{m,\varepsilon}$ can be observed as eccentricity increases.

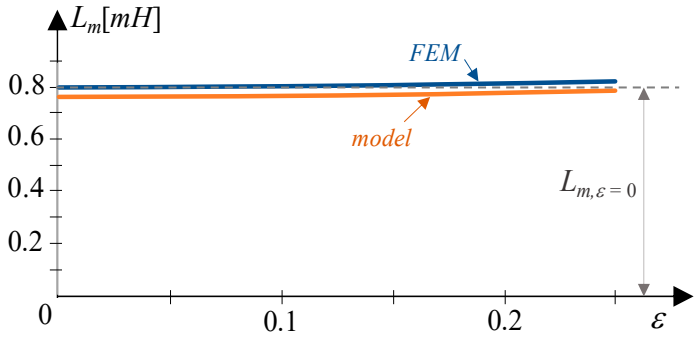

Figure 14. Air gap mutual inductance as a function of ε. Results of the model (brown line) and of FEM analysis (blue line).

7. Conclusions

By some geometrical considerations and a set of simplifying hypotheses, an analytical lumped-parameter model was derived for a surface-magnets PM motor affected by static eccentricity. The equations presented apply for a distributed 3-phase winding with only series connections between coils of a given phase. The analytical model was validated successfully through FEM analysis for a case-study in which sinusoidal currents were assumed to be impressed in the motor, as common for AC brushless motors fed with current-controlled voltage source inverters. The trends of the results show the goodness of the proposed analytical model: in fact, the difference in the magnitude of the considered electrical quantities is very low, and the spectra of FEM results and analytical model are coincident.

The numerical validation confirms the analytical model as an adequate mean to gain further insight into the effects of static eccentricity on the operation of the PM motors. These effects can be broadly summarized as follows.

Static eccentricity translates into magnetic anisotropy and thus introduces infinite additional harmonic components in the airgap flux-density distributions generated by stator currents and permanent magnets; the resulting spatial distributions are modulated and lose their periodicity along a double pole pitch.

Due to the assumed full-pitch armature winding and the series connection between phase coils, these additional spatial harmonics do not introduce in the linked fluxes and back e.m.f.s different harmonics from those already observable during healthy operation. Symmetric behavior in the three phases is preserved as well.

The eccentricity affects the values of some parameters in the model. In particular, the amplitude of the first harmonic of rotor flux experiences a little increase, resulting in a correspondent small increase in the mean value of the electromagnetic torque with respect to the healthy case. The mutual inductance is slightly increased as well. However, both variations appear rather modest.

These results suggest that, for the considered layout of the machine, static eccentricity cannot be easily detected through time or frequency inspection of the main electromagnetic variables. The highlighted variation in the machine parameters appears as the only potential indicator of the considered fault, although weak and hardly detectable in real applications.

Author Contributions: Conceptualization, A.D.P. and E.F.; methodology, A.D.P. and E.F.; software, L.P.D.N. and E.F.; validation, A.D.P., L.P.D.N. and E.F.; writing—original draft preparation, A.D.P., L.P.D.N. and E.F.; All authors have read and agreed to the published version of the manuscript.

Funding: This research was funded by the project "REINForce–REsearch to INspire the Future", funded by Italian Ministry M.I.S.E.

Conflicts of Interest: The authors declare no conflict of interest.

Appendix A. —Finite Element Analysis

The verification of the goodness of the analytical model is carried out through the comparison with finite element analysis. The analyses are performed using the software FEMM 4.2 [16]. The following appendix summarizes the modalities of calculation of back-e.m.f., phase armature voltage, electromagnetic torque and synchronous mutual inductance:

- *Calculation of back-e.m.f.*

The back-e.m.f. is calculated using the Faraday's law. The methodology needs the determination of the linkage flux with a single phase. For a 2-D problem, the linkage flux of a single-phase coil with massive conductor is calculated as [17,18]:

$$\Phi = \frac{L}{S_c}\left(\int_{S_c} A_z dS\Big|_{left} - \int_{S_c} A_z dS\Big|_{right}\right) \tag{A1}$$

where S_c is the conductor area, A_z is the z-component of the potential vector of magnetic flux density, L is the stack length of the motor. The integral in (A1) are computed both on left and right side of the phase coils. The numerical derivative of (A1) gives the back-emf.

- *Phase armature voltage*

The phase armature voltage [17,18] is calculated adding the voltage drop on the single-phase resistance to the back-e.m.f. The resistance is calculated through the evaluation of Joule losses.

- *Electromagnetic torque calculation*

The electromagnetic torque is calculated using the Maxwell stress tensor [17,18]. Considering a 2-D geometry, the expression is:

$$M_e = \frac{L}{\mu_0}\oint_{l_r} r B_n B_t \, dl \tag{A2}$$

where L is the magnetic stack length, r is the radius of an opportune contour l_r located in the airgap and around the rotor, while B_n and B_t are the normal and tangential components of magnetic flux density on the contour.

- *Synchronous mutual inductance*

The value of synchronous mutual inductance L_m is obtained by means of the calculation of electromagnetic energy E_{gap} in the airgap [17,18]. Eliminating the permanent magnet magnetization, the E_{gap} is calculated imposing a quadrature axis current of amplitude I_{max} (it was verified that with a d-axis current, the value of mutual inductance of the considered motor is the same). Therefore, the mutual inductance is equal to:

$$L_m = \frac{4}{3}\frac{E_{gap}}{I_{\max}^2} \tag{A3}$$

References

1. Nandi, S.; Bharadwaj, R.M.; Toliyat, H.A. Performance analysis of a three-phase induction motor under mixed eccentricity condition. *IEEE Trans. Energy Convers.* **2002**, *17*, 392–399. [CrossRef]
2. Dorrell, D.G.; Thomson, W.T.; Roach, S. Analysis of airgap flux, current, and vibration signals as a function of the combination of static and dynamic airgap eccentricity in 3-phase induction motors. *IEEE Trans. Ind. Appl.* **1997**, *33*, 24–34. [CrossRef]
3. Shakouhi, M.; Mohamadian, M.; Afjei, E. Fault-Tolerant Control of Brushless DC Motors under Static Rotor Eccentricity. *IEEE Trans. Ind. Electron.* **2015**, *62*, 1400–1409. [CrossRef]
4. Rajagopalan, S.; Roux, W.L.; Habetler, T.G.; Harley, R.G. Dynamic Eccentricity and Demagnetized Rotor Magnet Detection in Trapezoidal Flux (Brushless DC) Motors Operating Under Different Load Conditions. *IEEE Trans. Power Electron.* **2007**, *22*, 2061–2069. [CrossRef]
5. Veras, F.C.; Lima, T.L.V.; Souza, J.S.; Ramos, J.G.G.S.; Filho, A.C.L.; Brito, A.V. Eccentricity Failure Detection of Brushless DC Motors From Sound Signals Based on Density of Maxima. *IEEE Access* **2019**, *7*, 150318–150326. [CrossRef]
6. Goktas, T.; Zafarani, M.; Akin, B. Discernment of Broken Magnet and Static Eccentricity Faults in Permanent Magnet Synchronous Motors. *IEEE Trans. Energy Convers.* **2016**, *31*, 578–587. [CrossRef]
7. Faiz, J.; Ebrahimi, B.M.; Akin, B.; Toliyat, H.A. Comprehensive Eccentricity Fault Diagnosis in Induction Motors Using Finite Element Method. *IEEE Trans. Magn.* **2009**, *45*, 1764–1767. [CrossRef]
8. Ebrahimi, B.M.; Faiz, J.; Javan-Roshtkhari, M.; Nejhad, A.Z. Static Eccentricity Fault Diagnosis in Permanent Magnet Synchronous Motor Using Time Stepping Finite Element Method. *IEEE Trans. Magn.* **2008**, *44*, 4297–4300. [CrossRef]
9. Rahideh, A.; Korakianitis, T. Analytical Open-Circuit Magnetic Field Distribution of Slotless Brushless Permanent-Magnet Machines With Rotor Eccentricity. *IEEE Trans. Magn.* **2011**, *47*, 4791–4808. [CrossRef]
10. Alam, F.R.; Abbaszadeh, K. Magnetic Field Analysis in Eccentric Surface-Mounted Permanent-Magnet Motors Using an Improved Conformal Mapping Method. *IEEE Trans. Energy Convers.* **2016**, *31*, 333–344. [CrossRef]
11. Abdelli, R.; Bouzida, A.; Touhami, O.; Ouadah, M. Static eccentricty fault modeling in permanent-magnet synchronous motors. In Proceedings of the 8th International Conference on Modeling, Identification and Control (ICMIC), Algiers, Algeria, 15–17 November 2016.
12. Zhu, Z.Q.; Wu, L.J.; Jamil, M.L.M. Distortion of back-EMF and torque of PM brushless machines due to eccentricity. *IEEE Trans. Magn.* **2013**, *49*, 4927–4936. [CrossRef]
13. del Pizzo, A.; Marongiu, I.; Perfetto, A. Mathematical model of asynchronous machines in presence of constructive asymmetries. *L'Energia Elettrica* **1989**, *56*, 235–241.
14. del Pizzo, A.; Perfetto, A.; Marongiu, I. Mathematical model of asynchronous motors in presence of static eccentricity. *L'Energia Elettrica* **1990**, *57*, 41–48.
15. del Pizzo, A.; di Noia, L.P.; Fedele, E. An analytical evaluation of rotor eccentricity effects on synchronous drives with surface mounted permanent magnet brushless motors. In Proceedings of the IEEE-20th Mediterranean Electrotechnical Conference (MELECON 2020), Palermo, Italy, 16–18 June 2020.
16. Meeker, D.C. Finite Element Method Magnetics. Available online: http://www.femm.info (accessed on 1 July 2020).
17. Silvester, P.P.; Ferrari, R.L. *Finite Elements for Electrical Engineers*, 3rd ed.; Cambridge University Press: Cambridge, UK, 1996.
18. Salon, S.J. *Finite Element Analysis of Electrical Machines*; Kluwer Academic Publishers: Boston, MA, USA, 1995.